Local sympathetic neurons promote neutrophil egress from the bone marrow at the onset of acute inflammation

Tomoka Ao[1,2], Junichi Kikuta[1,2], Takao Sudo[1,2], Yutaka Uchida[1], Kenta Kobayashi[3] and Masaru Ishii[1,2]

[1]Department of Immunology and Cell Biology, Graduate School of Medicine and Frontier Biosciences, Osaka University, Osaka, Japan
[2]WPI-Immunology Frontier Research Center, Osaka University, Osaka, Japan
[3]Section of Viral Vector Development, National Institute for Physiological Sciences, National Institute of Natural Sciences, Aichi, Japan

Correspondence to
Masaru Ishii, Department of Immunology and Cell Biology, Graduate School of Medicine and Frontier Biosciences, Osaka University, 2-2 Yamada-oka, Suita, Osaka 565-0871, Japan
Email: mishii@icb.med.osaka-u.ac.jp
Tel: +81 6-6879-3880, Fax: +81 6-6879-3889
Junichi Kikuta, Department of Immunology and Cell Biology, Graduate School of Medicine and Frontier Biosciences, Osaka University, 2-2 Yamada-oka, Suita, Osaka 565-0871, Japan
Email: jkikuta@icb.med.osaka-u.ac.jp
Tel: +81 6-6879-3881, Fax: +81 6-6879-3889

Running title
Sympathetic neurons promote neutrophil egress

Keywords
neutrophil egress, intravital imaging, sympathetic neuron, endothelium, bone marrow

The total number of pages and figures
42 pages and 4 figures

ABSTRACT

The sympathetic nervous system plays critical roles in the differentiation, maturation, and recruitment of immune cells under homeostatic conditions, and in responses to environmental stimuli, although its role in the migratory control of immune cells during acute inflammation remains unclear. In this study, using an advanced intravital bone imaging system established in our laboratory, we demonstrated that the sympathetic nervous system locally regulates neutrophil egress from the bone marrow for mobilization to inflammatory foci. We found that sympathetic neurons were located close to blood vessels in the bone marrow cavity; moreover, upon lipopolysaccharide (LPS) administration, local sympathectomy delayed neutrophil egress from the bone marrow and increased the proportion of neutrophils that remained in place. We also showed that vascular endothelial cells produced C-X-C motif chemokine ligand 1 (CXCL1), which is responsible for neutrophil egress out of the bone marrow. Its expression was upregulated during acute inflammation, and was suppressed by β-adrenergic receptor blockade, which was accompanied with inhibition of neutrophil egress into the systemic circulation. Furthermore, systemic β-adrenergic signaling blockade decreased the recruitment of neutrophils in the lung under conditions of acute

systemic inflammation. Taken together, the results of this study first suggested a new regulatory system, wherein local sympathetic nervous activation promoted neutrophil egress by enhancing *Cxcl1* expression in bone marrow endothelial cells in a β-adrenergic signaling-dependent manner, contributing to the recruitment of neutrophils at the onset of inflammation *in vivo*.

Introduction

The sympathetic nervous system plays a critical role in maintaining homeostasis, and in the response to acute stress. Peripheral sympathetic neurons innervate all of the organs and exert their regulatory functions via local release of the neurotransmitter norepinephrine (NE). Recently, sympathetic neurons in bone marrow have been shown to have crucial functions. In the homeostatic state, they are involved in myelopoiesis through regulation of perivascular mesenchymal stromal cells, which synthesize various factors (e.g., stromal cell-derived factor 1 [SDF-1], C-X-C motif chemokine ligand 12 [CXCL12]) that promote the maintenance and/or localization of hematopoietic stem cells (1-4). Furthermore, it has been reported that sympathetic neurons govern circadian leukocyte recruitment to bone marrow through β2-adrenergic signaling (5). Under stressful conditions, including granulocyte colony-stimulating factor (G-CSF) treatment, hypertension, and exercise, sympathetic neurons are activated, induce downregulation of CXCL12 in mesenchymal stromal cells, and are involved in the recruitment of hematopoietic stem and progenitor cells (HSPCs) into the circulation (3,6,7). In addition to HSPCs, NE is known to regulate neutrophil dynamics. Injection of NE has been

shown to increase the number of circulating neutrophils (8,9). Therefore, sympathetic neurons are assumed to play a role in neutrophil trafficking.

Neutrophils are major players in acute inflammation and are essential for eradication of bacterial infections. However, excessive accumulation of neutrophils can be detrimental to the host (10,11). Neutrophils arise from hematopoietic stem cells in bone marrow, where they spend the majority of their life; under physiological conditions, more than 98% of neutrophils are found in bone marrow (12). In response to infection, large numbers of neutrophils are recruited to affected tissues, and mature neutrophils are mobilized from the bone marrow into the circulation to compensate for their peripheral loss. As neutrophil mobilization is the most crucial step in host defense against tissue injury under conditions of acute inflammation, the mechanisms underlying neutrophil regulation have been studied in detail. The most notable neutrophil-mobilizing factors are keratinocyte chemoattractant (KC; C-X-C-motif ligand 1 [CXCL1]) and macrophage inflammatory protein 2 (MIP-2; CXCL2), which are ligands for C-X-C motif chemokine receptor 2 (CXCR2). In contrast, SDF-1 (CXCL12) expressed on stromal cells, which is a ligand for CXCR4, and vascular cell

adhesion molecule 1 (VCAM-1), which is a ligand for very late antigen 4 (VLA-4), retain neutrophils in the bone marrow (13-19). G-CSF, a major neutrophil-mobilizing factor, mobilizes neutrophils by reducing the levels of CXCL12 in bone marrow, and CXCR4 expression on neutrophils (12,17,20). However, the contribution of sympathetic regulation to neutrophil egress, which is the most critical process during the onset of acute inflammation, remains unclear.

We hypothesized that sympathetic neurons regulate neutrophil egress via the chemotactic environment at the onset of acute inflammation. In most conventional studies, 6-hydroxydopamine (6OHDA) or pharmacological agents have been used to examine systemic sympathetic regulation (2,3,21). However, local sympathetic regulation cannot be analyzed due to the inability to directly monitor neutrophil egress, including cellular movement in narrow areas.

In recent years, the development of optical imaging techniques has allowed us to obtain a better understanding of cellular dynamics within tissues (18,22,23). Here, we established a novel local sympathectomy approach, and evaluated the role of local sympathetic neurons in the motility of neutrophils in the bone marrow of living mice.

Intravital bone imaging showed that neutrophil egress was suppressed in denervated bone marrow in the early phase of inflammation. Furthermore, we demonstrated that β-adrenergic receptor blockade suppressed the neutrophil egress and attenuated the accumulation of neutrophils in the lung.

Materials and Methods

Animals

C57BL/6 mice were purchased from Japan Clea (Tokyo, Japan). Mice with targeted insertion of enhanced green fluorescent protein (EGFP) in the lysozyme-M (LysM) locus (LysM-EGFP mice) were also used (24). The mice were males aged 8–12 weeks. For intravital imaging experiments, bone marrow chimeras were generated by irradiating 6-week-old recipient mice with a single dose of 10 Gy using Gammacell 40 (Atomic Energy of Canada Ltd., Ottawa, Canada), followed by intravenous transfer of bone marrow cells. Donor bone marrow cells consisted of 0.5×10^6 LysM-EGFP mouse-derived cells and 4.5×10^6 wild-type mouse-derived cells. Chimeras were analyzed at least 8 weeks after irradiation. All mice were housed at a maximum of six animals per cage; mice were randomly selected for the experiments. All mice were maintained under a 12-hour/12-hour light/dark cycle in the specific pathogen-free animal facilities of Osaka University. Considering the circadian oscillation of sympathetic activity, the experiments were performed during the light cycle (between 10:00 and 19:00). All animal experiments were approved by the Institutional Animal Experimental Committee of Osaka University.

Treatment with drugs

For the acute inflammation model, lipopolysaccharide (LPS) (10 mg/kg; Sigma-Aldrich, St. Louis, MO, USA) dissolved in phosphate-buffered saline (PBS; Nacalai Tesque, Kyoto, Japan) was injected intraperitoneally. Propranolol (15 mg/kg; Sigma-Aldrich) dissolved in saline was injected intraperitoneally 30 minutes before LPS administration.

Isolation of bone endothelial cells

Bone endothelial cells and mesenchymal cells were prepared as reported previously (25). Briefly, femurs, tibia, and hip bones were crushed and incubated in 3 mg/mL of collagenase type I (Worthington Biochemical Corp, Freehold, NJ, USA) in HBSS(+) (Nacalai Tesque) at 37°C for 60 minutes, and then filtered. Red blood cells were eliminated using ACK Lysing Buffer (Thermo Fisher Scientific, Waltham, MA, USA). After single-cell suspension, cells were incubated in Fc-block (2.4G2) (BD Biosciences, San Jose, CA, USA) for 10 minutes on ice, and then incubated with a cocktail of

biotin-conjugated antibodies to lineage-specific markers (CD5, CD11b, CD45R/B220, Gr-1, 7-4, Ter119) (Miltenyi Biotec, Bergisch Gladbach, Germany) for 20 minutes, followed by staining with FITC-conjugated anti-CD31 antibody (390) (BD Biosciences), PerCPCy5.5-conjugated anti-streptavidin antibody (eBioscience, San Diego, CA, USA), APC-conjugated anti-CD45 antibody (30-F11; BioLegend, San Diego, CA, USA), and PE-Cy7-conjugated anti-Sca1 antibody (D7; BD Biosciences) or isotype control antibody (RTK2758; BioLegend). Cells were isolated using a cell sorter (Sony, Tokyo, Japan) and the data were analyzed using FlowJo software (TreeStar, Ashland, OR, USA).

Endothelial cell culture and gene expression analysis

Human umbilical vein endothelial cells (HUVECs) purchased from KURABO (Osaka, Japan) were cultured in Endothelial Basal Medium-2 basal medium supplemented with the Endothelial Cell Growth Medium-2 BulletKit (Lonza, Basel, Switzerland). The cells used in the experiments were cultured up to passage 10. Cells were cultured in RPMI (Nacalai Tesque) supplemented with 2% heat-inactivated fetal

bovine serum (Sigma-Aldrich) for 4 hours prior to the experiment. Aliquots of 1×10^5 HUVECs were grown in 24-well plates and treated with 100 μM isoproterenol (Sigma-Aldrich) in the presence or absence of LPS (1 ng/mL), and 2 hours later, the expression of *Cxcl1* was analyzed by quantitative real-time PCR.

Bone marrow cell preparation and flow cytometry

Bone marrow cells from femurs were isolated by flushing. Cells from parietal bones were isolated by gently crushing in a mortar. After a single-cell suspension was obtained, cells were incubated in Fc-block (2.4G2; BD Biosciences) for 10 minutes on ice, and stained with FITC-conjugated anti-CD45 antibody (30-F11; BioLegend), APC-conjugated anti-Ly6G antibody (1A8; BioLegend), and BV421-conjugated anti-CD11b antibody (M1/70; BioLegend). Cells were analyzed by flow cytometry (FACS Canto II; BD Biosciences) and the data were analyzed using FlowJo software.

Analysis of neutrophils in whole blood cells

To determine the number of circulating neutrophils, peripheral blood was collected by cardiac puncture from mice anesthetized with 2% isoflurane (Fujifilm Wako Pure

Chemical Corporation, Osaka, Japan). The number of neutrophils was counted by microscopic examination (Fujifilm Wako Pure Chemical Corporation).

Biochemical analysis

To determine the plasma adrenocorticotropic hormone (ACTH) and corticosterone levels, peripheral blood was collected at 11:00 from sham-operated or sympathectomized mice 2 hours after PBS or LPS administration. Whole blood was mixed with EDTA and centrifuged for 15 minutes at 1000 × *g*, and the supernatant plasma was used for enzyme-linked immunosorbent assay (ELISA) using commercial kits (MyBioSource, San Diego, CA, USA for ACTH and Enzo Life Sciences, New York, NY, USA for corticosterone) according to the manufacturer's instructions.

Quantitative real-time PCR

Total RNA and cDNA were prepared using the RNeasy micro kit (Qiagen, Hilden, Germany) and Superscript III reverse transcriptase (Thermo Fisher Scientific) according to the manufacturers' instructions. Real-time PCR analysis was performed with a

Thermal Cycler Dice Real Time system (TaKaRa, Shiga, Japan) using SYBR Premix EX Taq (Tli RNaseH Plus; TaKaRa). Gene expression values were calculated by the ΔΔCt method using *Gapdh* (for murine cells) or *ACTB* (for human cells) as an internal control. The primers used for the assay are listed in Supplementary Table 1.

Immunohistochemistry of frozen sections

Parietal bone tissues were harvested 10 days after sympathectomy. For immunohistochemical analysis of CXCL1, PBS or LPS was injected intraperitoneally 2 hours prior to collection. To prepare parietal bone sections, mice were perfused with 4% (v/v) paraformaldehyde (PFA; Sigma-Aldrich), and dissected bone tissues were fixed in 4% PFA for 30 minutes at room temperature, followed by washing three times with PBS for 10 minutes each time. The fixed samples were embedded in Super Cryoembedding medium (Section-LAB, Hiroshima, Japan). Then, 10-μm-thick sections were prepared using the Kawamoto film method, blocked, and stained in Dako REAL Antibody Diluent (Dako, Glostrup, Denmark) containing the following primary antibodies at 4°C overnight: anti-tyrosine hydroxylase (TH; AB152; Millipore, Burlington, MA, USA), anti-CD105 (MJ7/18; BioLegend), and anti-CXCL1 (ab86436;

Abcam, Cambridge, UK) antibodies. Following this, they were stained with anti-rabbit IgG Alexa Fluor 488-conjugated secondary antibody (Thermo Fisher Scientific) and anti-rat IgG Alexa Fluor 647-conjugated secondary antibody (Jackson ImmunoResearch, West Grove, PA) for 40 minutes at room temperature. Sections were mounted with Fluoromount (Diagnostic BioSystems, Pleasanton, CA, USA) or VECTASHIELD mounting medium with 4′,6-diamidino-2-phenylindole (DAPI; Vector Laboratories, Burlingame, CA, USA).

Lungs were harvested 2 hours after LPS/PBS treatment. LysM-EGFP mice were perfused with 4% PFA, and lung tissues were dissected and embedded in optimal cutting temperature (OCT) compound (Sakura Fine Tek Japan, Tokyo, Japan). Vessels were visualized by intravenous injection of anti-CD31 Alexa Fluor 647-conjugated antibody (MEC13.3; BioLegend) 15 minutes before perfusion. Then, 10-μm-thick sections were prepared and mounted with Fluoromount.

Sympathetic ganglia were exposed and perfused with 4% PFA followed by dissection. The fixed samples were embedded in OCT compound. Then, 10-μm-thick sections were prepared, blocked, and stained in Dako REAL Antibody Diluent

containing anti-TH antibody or anti-c-Fos antibody (E-8; Santa Cruz Biotechnology, Dallas, TX, USA) at 4°C overnight and subsequently stained with anti-mouse IgG1 Alexa Fluor 488-conjugated secondary antibody (Thermo Fisher Scientific) or anti-rabbit IgG Alexa Fluor 594-conjugated secondary antibody for 30 minutes at room temperature. Sections were mounted with VECTASHIELD mounting medium with DAPI.

All samples were frozen in chilled hexane (Fujifilm Wako Pure Chemical Corporation) using dry ice and cut into sections using a cryostat (CM3050; Leica, Wetzlar, Germany). All sections were examined by confocal microscopy (A1; Nikon, Tokyo, Japan) illuminated with a laser (wavelength: 405 nm for DAPI, 488 nm for EGFP and Alexa Fluor 488, 561 nm for Alexa Fluor 594, and 638 nm for Alexa Fluor 647). Bone tissues were visualized under transmitted light. Image stacks were collected (3-μm vertical step size) and maximum intensity projection (MIP) images were generated before evaluation.

Intravital imaging

Mouse parietal bone tissues were examined via intravital microscopy using a modified version of a protocol reported previously (26). Briefly, mice were anesthetized with 2% isoflurane, and the frontoparietal skull bone was surgically exposed and immobilized. The parietal bone marrow was observed by two-photon microscopy. During imaging, mice were anesthetized with < 1% isoflurane plus 1.4 mg/kg of urethane (Sigma-Aldrich). Mice were cannulated and vessels were visualized by continuous intravenous injection of Qtracker 655 (Thermo Fischer Scientific) using a syringe pump (KDS 100; LMS, Tokyo, Japan) during imaging. Intravital bone imaging experiments were performed using an upright two-photon microscope (A1R-MP; Nikon) equipped with a 25× water-immersion objective (APO: numerical aperture [NA], 1.1; Nikon). The system was driven by a femtosecond-pulsed infrared laser (Chameleon Vision II Ti:Sapphire; Coherent, Santa Clara, CA, USA). Fluorescence was detected by an external non-descanned detector (NDD; Nikon) with the following emission filters: 492/SP nm for the second harmonic generation (SHG), 525/50 nm for EGFP, and 629/56 nm for Qtracker 655. Image stacks were collected with a 5-μm vertical step size to a depth of 65 μm below the skull bone surface. The time resolution was 40 seconds

for tracking and the interval of observation was 30 minutes for counting cells in the visual field. Acquired raw images were subjected to channel unmixing with NIS Elements software (Nikon), to create unmixed images that excluded autofluorescence.

Analysis of intravital imaging data

Regarding cell trajectories, 3D imaging data were processed to generate MIP images using NIS Elements software. The 2D data were processed using Imaris (Bitplane, Belfast, UK) software; automatic 2D object tracking with the Imaris spot-detection algorithm was assisted by manual adjustment, and we retrieved cell coordinates over time. Cells flowing in blood vessels were excluded manually from the analysis. To count the cells in the visual field, automatic 3D object segmentation with the Imaris spot-detection algorithm was used. An egress event was defined as a cell overlapping with a vessel in an image frame, but not in the next frame. The time of an egress event was determined manually.

Tracing superior cervical ganglion (SCG) neurons with adeno-associated viruses (AAVs)

Mice were anesthetized with isoflurane (2%). A ventral neck incision was made to identify the carotid bifurcation. After the carotid artery was turned over, the SCG was exposed. An AAV (serotype DJ) encoding AAV-CAGGS-EGFP-WPRE (1.0×10^{12} copies/mL, 250–500 nL) was injected into each side of the SCG at a rate of 150 nL/mL using an Ultra micropump-III (WPI, Sarasota, FL, USA) equipped with a syringe (Hamilton, Reno, NV, USA) connected to a glass capillary. The syringe was filled with Fluorinert (3M, St. Paul, MN, USA). The parietal bone and SCG were observed using an upright two-photon microscope and confocal microscope, respectively, 2 weeks after AAV injection.

Superior cervical ganglionectomy (SCGx)

Mice were operated on as described previously, under anesthesia with isoflurane (2%) (5). A ventral neck incision was made to identify the carotid bifurcation. The SCG and sympathetic trunk were transected bilaterally. After the surgical procedure, mice

were housed under normal conditions. Intravital imaging, flow cytometry, and immunohistochemistry were performed 10 days after the operation. Assessment of sympathetic nerve ablation was performed by immunohistochemical analysis of vessels at the center of parietal bones. Using NIS Elements software, the $CD105^+$ perivascular area was cropped and the TH^+ area was measured on cropped images. The sympathectomized group and sham-operated group were then compared.

Statistics

The results are presented as means; error bars indicate SEM. The Mann–Whitney rank sum test was performed using GraphPad PRISM software (GraphPad Software Inc., San Diego, CA, USA) to calculate *P*-values for highly skewed distributions. For Gaussian-like distributions, the two-tailed *t* test was used. For all other cases, the methods used are described in the corresponding figures. In all analyses, $P < 0.05$ was taken to indicate statistical significance.

Results

Establishment of an intravital imaging system for visualization of the local function of sympathetic neurons in bone marrow

To investigate local sympathetic regulation in bone marrow, we established a local sympathectomy-based approach combined with intravital bone imaging. As the SCG is the largest sympathetic ganglion located at the top of the sympathetic chain, and because neurons derived from the SCG cover most of the calvarium, we first examined the location where SCG neurons innervate in the parietal bone marrow. We locally injected AAV vectors carrying EGFP into the SCG (Supplementary Figures 1A and B). Intravital two-photon imaging allowed visualization of innervation in detail; the nerve terminals were adjacent to the blood vessels (Supplementary Figure 1C). Next, to examine the function of sympathetic neurons, we performed bilateral SCGx (Supplementary Figure 1D). In histological analysis, TH signals around vessels were shown to be completely ablated 10 days after sympathectomy (Supplementary Figure 1E). As plasma ACTH was reported to be affected by sympathectomy in rats (27), we confirmed that bilateral sympathectomy did not interfere with the plasma levels of

stress-related hormones, including ACTH and corticosterone, with or without LPS administration (Supplementary Figure 1F). This approach allowed us to investigate the role of local innervation.

Intravital two-photon microscopy of mice carrying a targeted insertion of EGFP in the LysM locus can visualize neutrophil migration in bone marrow (18,22,24). However, the neutrophil density is too high to assess motility at the single-cell level. Therefore, we generated bone marrow chimeric mice to reduce the density of fluorescently labeled cells in the bone marrow: 10% of donor cells were derived from LysM-EGFP mice, and 90% were derived from wild-type mice. SCGx did not affect the motility of neutrophils in the homeostatic state (Supplementary Figures 1G, H, and Supplementary Video 1).

Neutrophil egress out of bone marrow in LPS-induced acute inflammation

Sympathetic neurons are activated under conditions of acute stress (28,29). LPS administration has been reported to increase the hypothalamic synthesis of tumor necrosis factor-α and cyclooxygenase-2 and to induce prostaglandin E2 synthesis, resulting in the firing of neurons in the rostral ventrolateral medulla and paraventricular

nucleus, as well as peripheral sympathetic nerve activation (30-32). To examine the function of SCG neurons in acute inflammation, we induced acute inflammation by intraperitoneal injection of LPS. Intravital imaging of bone marrow in chimeric mice showed that neutrophils egressed from bone marrow into the circulation (Supplementary Figures 2A and B). In addition, LPS treatment significantly reduced the number of neutrophils and increased their velocity compared to the non-stimulated state (Supplementary Figures 2B–D). The reduction persisted for up to 120 minutes; at that time, there were 72% fewer neutrophils than at time 0, with the number then remaining constant up to 180 minutes (Supplementary Figure 2C). In accordance with these results, the observation period was set as up to 120 minutes in the following experiments. The reduction in cellularity was accompanied by marked elevation in neutrophil velocity, which reached > 3 μm/minutes within 120 minutes (Supplementary Figure 2D). Furthermore, we confirmed that the number of SCG neurons expressing c-Fos was increased after LPS treatment, indicating activation of peripheral sympathetic neurons innervating the parietal bone marrow (Supplementary Figure 2E). We also examined the LPS-induced reduction of $Ly6G^+$ $CD11b^+$ bone marrow neutrophils by flow cytometry

in both femoral bone and parietal bone (Supplementary Figures 2F and 3C). In addition, the number of circulating neutrophils did not increase during the imaging period because they accumulated in peripheral organs (Supplementary Figure 2G).

Neutrophil egress after LPS treatment was impaired in denervated bone marrow

To assess the local sympathetic regulation of acute inflammation, we compared the number, velocity, and egress events of neutrophils between the sham-operated group and sympathectomized group after LPS administration. We found that the reduction in number of neutrophils was less marked in the sympathectomized group than the sham-operated group. At 90 minutes, the number of remaining neutrophils in the sympathectomized group was twice that in the sham-operated group; a significant difference was also observed at 120 minutes (Figs. 1A and B). In addition, the mean velocity of neutrophils in the sympathectomized group was consistently lower than that in the sham-operated group throughout the imaging period (Supplementary Figures 3A, B and Supplementary Video 3). Furthermore, we also determined when neutrophil egress occurred during the 120-minute observation period. The mean time of occurrence

shifted from 54.6 ± 1.9 to 60.5 ± 1.8 minutes after sympathectomy, indicating that sympathetic neurons can promote rapid egress of neutrophils from the bone marrow (Fig. 1C). The inhibitory effects of sympathectomy on the number and frequency of neutrophils in parietal bone marrow were also examined by flow cytometry (Supplementary Figure 3C). Sympathectomy did not affect the number or frequency of neutrophils after PBS treatment. In contrast, after LPS treatment, the number and frequency of neutrophils were significantly more in denervated bone marrow compared with sham-operated bone marrow. These results suggested that local sympathetic regulation positively contributes to neutrophil egress from the bone marrow into the circulation by causing rapid transmigration under conditions of LPS-induced acute inflammation.

β-adrenergic inhibitor suppressed the expression of Cxcl1 in endothelial cells

The mechanism of neutrophil mobilization from bone marrow to the circulation has been explained by the “tug of war” model. The CXCR2 ligands CXCL1 and CXCL2 influx from the vessel side and induce neutrophil chemotaxis into the circulation, while

CXCL12 expressed by mesenchymal stromal cells promotes neutrophil retention (13-18). As sympathetic neurons were found to be in contact with blood vessels (Supplementary Figure 1C), we hypothesized that these neurons may modulate the production of CXCL1 or CXCL2 by endothelial cells, resulting in the induction of neutrophil mobilization. Endothelial cells, megakaryocytes, and osteoblasts have all been reported as sources of CXCL1 and CXCL2 (15,22); we found that Lin^- $CD45^-$ $CD31^+$ $Sca\text{-}1^+$ endothelial cells had higher *Cxcl1* expression level compared to Lin^- $CD45^-$ stromal cells and $CD45^+$ leukocytes. In addition, LPS upregulated the expression of *Cxcl1*, whereas upregulation of *Cxcl2* was limited (Figs. 2A and B); this suggested that CXCL1 produced by endothelial cells is an important candidate regulator of neutrophil egress in LPS-induced inflammation.

Recent studies have reported the therapeutic effects of β-adrenergic inhibitors in sepsis models. For example, Wilson *et al.* and Özyılmaz *et.al.* reported that treatment with the β inhibitor, propranolol, attenuated lung injury and promoted survival in a cecal ligation and puncture (CLP) model of polymicrobial septic peritonitis (33,34). Next, we investigated the type of adrenergic receptors involved in signal transduction

from sympathetic neurons. Adrenergic receptors are classified into nine subtypes according to their pharmacological characteristics. We confirmed that bone marrow endothelial cells express mainly β2-adrenergic receptors, suggesting that sympathetic neurons regulate endothelial cells via β2-adrenergic signaling (Fig. 2C). To examine whether CXCL1 production in endothelial cells is mediated by β-adrenergic receptor signaling, we treated HUVECs with the β-adrenergic agonist isoproterenol in the presence or absence of LPS and measured *Cxcl1* expression. The level of *Cxcl1* expression was increased significantly only in the absence of LPS, indicating that β-adrenergic signaling promotes *Cxcl1* expression in the slight inflammatory stimuli (Supplementary Figure 4A). Furthermore, to examine the role of β-adrenergic signaling *in vivo*, we treated mice with propranolol prior to LPS administration, and analyzed gene expression in endothelial cells. The *Cxcl1* expression level was markedly suppressed by propranolol treatment (Fig. 2D). We also confirmed that upregulation of CXCL1 in endothelial cells under LPS treatment was attenuated after sympathectomy (Supplementary Figure 4B). Taken together, these results suggest that β2-adrenergic signaling mediates *Cxcl1* expression in endothelial cells.

β-adrenergic inhibitor suppressed egress of neutrophils and attenuated their accumulation in the lung

We next assessed the effects of propranolol on neutrophil motility. Intravital imaging analysis showed that propranolol pretreatment inhibited the reduction in neutrophil number to a similar extent to sympathectomy; more than 60% of neutrophils remained at 90 minutes, while 43% of neutrophils remained after vehicle pretreatment (Figs. 3A and B). We also determined when neutrophil egress occurred during the 120-minute observation. The mean time of occurrence shifted from 60.3 ± 2.6 minutes to 75.8 ± 2.4 minutes after propranolol pretreatment (Fig. 3C). Unlike the case of sympathectomy, there were no differences in the velocity of neutrophils throughout the imaging period (Supplementary Figure 5B). However, intravital imaging showed that the tracks of neutrophils after propranolol treatment were winding, whereas those after vehicle treatment were relatively straight (Supplementary Figure 5A, Supplementary Video 4). Neutrophils in the propranolol-treated bone marrow maintained their velocity and moved around the blood vessels but did not egress from the bone marrow. Taken

1 together, these results suggest that β-adrenergic signaling promotes rapid neutrophil
2 egress via interference with vessel-oriented migration of neutrophils.

3 In the LPS-induced acute inflammation model, large numbers of neutrophils did not
4 remain in the systemic circulation (Supplementary Figure 2G), indicating that mobilized
5 neutrophils accumulated in several organs in addition to the peripheral blood. The lung
6 is known to be the organ showing the highest neutrophil accumulation in sepsis (35,36).
7 We observed that propranolol pretreatment reduced neutrophil accumulation in lung
8 tissue (Fig. 3D), suggesting that blockade of β-adrenergic signaling could ameliorate
9 lung injury.

10

Discussion

A critical role of the sympathetic nervous system in immune cell control has not been clearly demonstrated, partly because conventional studies, such as those using pharmacological agents, have assessed the contributions of both endocrine and neuronal factors rather than the exclusive contribution of the local sympathetic nervous system. Here, using a new approach based on local sympathectomy and intravital imaging, we unequivocally revealed the impact of local sympathetic neurons on neutrophil dynamics *in vivo*.

Previous reports on circadian oscillation showed that sympathetic neurons recruit immune cells into the bone marrow, mediated by changes in the expression of endothelial selectins and integrins under homeostatic conditions (5). In contrast, we showed that sympathetic neurons recruited neutrophils into the circulation under conditions of LPS-induced acute inflammation; under emergency conditions, this seems reasonable because sympathetic neurons are involved in the fight or flight response.

We suggested that endothelial cell-derived CXCL1 contributed to sympathetic neuron-mediated neutrophil egress. However, several factors that induce neutrophil

egress, including CXCL1 and CXCL2, are not only produced from bone marrow, but are also produced by macrophages at sites of infection; these factors flow into the systemic circulation (37). As intravenous injection of these factors has been shown to markedly mobilize neutrophils (17,38), they seem to also be responsible for neutrophil egress. Further studies are needed to determine how sympathetic neurons can control the circulating factors.

We showed that sympathectomy and propranolol treatment caused similar effect on egress times and numbers of bone marrow neutrophils. This result exhibited that most of the β-adrenergic inputs was derived from sympathetic neurons rather than humoral inputs.

In this study, we focused on the function of CXCL1 as a neutrophil chemotactic signal, not on CXCL12 as a retention signal. It has been reported that activation of the sympathetic nervous system can downregulate osteoblast-derived CXCL12, resulting in the mobilization of HSPCs (3). Sympathetic innervation to osteoblasts was also observed other than that to blood vessels (39,40). Our preliminary experiment showed that the area occupied by osteoblasts was significantly increased in the calvarium after

sympathectomy. Therefore, it is possible that sympathectomy enhances the differentiation of osteoblasts expressing CXCL12, resulting in abundant retention signals for neutrophils in the bone marrow.

The heart rate was reported to be elevated during the first 10 minutes in cases of acute inflammation (29), indicating that sympathetic activation occurs within several minutes. The data shown in Fig. 1 indicated that the mean time of neutrophil egress events was approximately 60 minutes after LPS administration, and retardation of neutrophil egress occurred in the sympathectomized condition. This was consistent with the observation that sympathectomy inhibited the reduction in the number of neutrophils remaining in the bone marrow, particularly from 60 to 120 minutes after LPS stimulation. These observations suggest that the sympathetic neurons are activated in the early phase of acute inflammation and enhance the production of CXCL1 in endothelial cells, resulting in neutrophil egress from the bone marrow to the blood vessels. Further studies are required to determine the impact of sympathectomy on neutrophil movement, including directionality or transmigration.

Here, we suggested that local sympathetic neurons influenced the expression of *Cxcl1* in endothelial cells via β-adrenergic signaling, promoting neutrophil egress into the circulation in the early stage of acute inflammation (Fig. 4). Our intravital imaging approach could be utilized to further investigate the mechanism of local sympathetic regulation in bone marrow and provide insights into the anti-inflammatory effects of β-adrenergic inhibitors.

Funding

This work was supported by funding from CREST, Japan Science and Technology Agency (to M.I.); Grants-in-Aid for Scientific Research (S) from the Japan Society for the Promotion of Science (JSPS to M.I.); funding from PRIME (Japan Agency for Medical Research and Development [AMED] to J.K.); a Grant-in-Aid for Young Scientists from JSPS (to J.K.); and grants from the Uehara Memorial Foundation (to M.I.) the Kanae Foundation for the Promotion of Medical Sciences (to M.I.); Mochida Memorial Foundation (to M.I.); and the Takeda Science Foundation (to M.I.).

Author Contributions

T.A and M.I. conceived the study. T.A and J.K designed the experiments. T.A. performed the imaging experiments and data analysis, with the assistance of J.K., T.S., and Y.U.. K.K. contributed to the generation of the AAV vectors. T.A. wrote the initial draft. J.K., T.S., and M.I. revised the final draft.

References

1 Méndez-Ferrer, S., Michurina, T. V., Ferraro, F. *et al.* 2010. Mesenchymal and haematopoietic stem cells form a unique bone marrow niche. *Nature* 466:829.

2 Méndez-Ferrer, S., Lucas, D., Battista, M., and Frenette, P. S. 2008. Haematopoietic stem cell release is regulated by circadian oscillations. *Nature* 452:442.

3 Katayama, Y., Battista, M., Kao, W. M. *et al.* 2006. Signals from the sympathetic nervous system regulate hematopoietic stem cell egress from bone marrow. *Cell* 124:407.

4 Morrison, S. J. and Scadden, D. T. 2014. The bone marrow niche for haematopoietic stem cells. *Nature* 505:327.

5 Scheiermann, C., Kunisaki, Y., Lucas, D. *et al.* 2012. Adrenergic nerves govern circadian leukocyte recruitment to tissues. *Immunity* 37:290.

6 Al-Sharea, A., Lee, M. K. S., Whillas, A. *et al.* 2019. Chronic sympathetic driven hypertension promotes atherosclerosis by enhancing hematopoiesis. *Haematologica* 104:456.

7 Agha, N. H., Baker, F. L., Kunz, H. E. *et al.* 2018. Vigorous exercise mobilizes CD34+ hematopoietic stem cells to peripheral blood via the β. *Brain Behav Immun* 68:66.

8 Dhabhar, F. S., Malarkey, W. B., Neri, E., and McEwen, B. S. 2012. Stress-induced redistribution of immune cells--from barracks to boulevards to battlefields: a tale of three hormones--Curt Richter Award winner. *Psychoneuroendocrinology* 37:1345.

9 Ince, L. M., Weber, J., and Scheiermann, C. 2018. Control of leukocyte trafficking by stress-associated hormones. *Front Immunol* 9:3143.

10 Bardoel, B. W., Kenny, E. F., Sollberger, G., and Zychlinsky, A. 2014. The balancing act of neutrophils. *Cell Host Microbe* 15:526.

11 Kruger, P., Saffarzadeh, M., Weber, A. N. *et al.* 2015. Neutrophils: Between host defence, immune modulation, and tissue injury. *PLoS Pathog* 11:e1004651.

12 Semerad, C. L., Liu, F., Gregory, A. D., Stumpf, K., and Link, D. C. 2002. G-CSF is an essential regulator of neutrophil trafficking from the bone marrow to the blood. *Immunity* 17:413.

13 Burdon, P. C., Martin, C., and Rankin, S. M. 2005. The CXC chemokine MIP-2 stimulates neutrophil mobilization from the rat bone marrow in a CD49d-dependent manner. *Blood* 105:2543.

14 Martin, C., Burdon, P. C., Bridger, G., Gutierrez-Ramos, J. C., Williams, T. J., and Rankin, S. M. 2003. Chemokines acting via CXCR2 and CXCR4 control the release of neutrophils from the bone marrow and their return following senescence. *Immunity* 19:583.

15 Eash, K. J., Greenbaum, A. M., Gopalan, P. K., and Link, D. C. 2010. CXCR2 and CXCR4 antagonistically regulate neutrophil trafficking from murine bone marrow. *J Clin Invest* 120:2423.

16 Delano, M. J., Kelly-Scumpia, K. M., Thayer, T. C. *et al.* 2011. Neutrophil mobilization from the bone marrow during polymicrobial sepsis is dependent on CXCL12 signaling. *J Immunol* 187:911.

17 Wengner, A. M., Pitchford, S. C., Furze, R. C., and Rankin, S. M. 2008. The coordinated action of G-CSF and ELR+CXC chemokines in neutrophil mobilization during acute inflammation. *Blood* 111:42.

18 Bajrami, B., Zhu, H., Kwak, H. J. *et al.* 2016. G-CSF maintains controlled neutrophil mobilization during acute inflammation by negatively regulating CXCR2 signaling. *J Exp Med* 213:1999.

19 Petty, J. M., Lenox, C. C., Weiss, D. J., Poynter, M. E., and Suratt, B. T. 2009. Crosstalk between CXCR4/stromal derived factor-1 and VLA-4/VCAM-1 pathways regulates neutrophil retention in the bone marrow. *J Immunol* 182:604.

20 Kim, H. K., De La Luz Sierra, M., Williams, C. K., Gulino, A. V., and Tosato, G. 2006. G-CSF down-regulation of CXCR4 expression identified as a mechanism for mobilization of myeloid cells. *Blood* 108:812.

21 Lucas, D., Scheiermann, C., Chow, A. *et al.* 2013. Chemotherapy-induced bone marrow nerve injury impairs hematopoietic regeneration. *Nat Med* 19:695.

22 Köhler, A., De Filippo, K., Hasenberg, M. *et al.* 2011. G-CSF-mediated thrombopoietin release triggers neutrophil motility and mobilization from bone marrow via induction of Cxcr2 ligands. *Blood* 117:4349.

23 Devi, S., Wang, Y., Chew, W. K. *et al.* 2013. Neutrophil mobilization via plerixafor-mediated CXCR4 inhibition arises from lung demargination and blockade of neutrophil homing to the bone marrow. *J Exp Med* 210:2321.

24 Faust, N., Varas, F., Kelly, L. M., Heck, S., and Graf, T. 2000. Insertion of enhanced green fluorescent protein into the lysozyme gene creates mice with green fluorescent granulocytes and macrophages. *Blood* 96:719.

25 Schepers, K., Hsiao, E. C., Garg, T., Scott, M. J., and Passegué, E. 2012. Activated Gs signaling in osteoblastic cells alters the hematopoietic stem cell niche in mice. *Blood* 120:3425.

26 Matsuura, Y., Kikuta, J., Kishi, Y. *et al.* 2018. visualisation of different modes of action of biological DMARDs inhibiting osteoclastic bone resorption. *Ann Rheum Dis* 77:1219.

27 Romeo, H. E., Spinedi, E., Vacas, M. I., Estivariz, F., and Cardinali, D. P. 1990. Increase in adrenocorticotropin release during wallerian degeneration of peripheral sympathetic neurons after superior cervical ganglionectomy of rats. *Neuroendocrinology* 51:213.

28 Annane, D., Trabold, F., Sharshar, T. *et al.* 1999. Inappropriate sympathetic activation at onset of septic shock: a spectral analysis approach. *Am J Respir Crit Care Med* 160:458.

29 Masson, G. S., Nair, A. R., Dange, R. B., Silva-Soares, P. P., Michelini, L. C., and Francis, J. 2015. Toll-like receptor 4 promotes autonomic dysfunction, inflammation and microglia activation in the hypothalamic paraventricular nucleus: role of endoplasmic reticulum stress. *PLoS One* 10:e0122850.

30 Zhang, Z. H., Yu, Y., Wei, S. G., and Felder, R. B. 2010. Centrally administered lipopolysaccharide elicits sympathetic excitation via NAD(P)H oxidase-dependent mitogen-activated protein kinase signaling. *J Hypertens* 28:806.

31 Zhang, Z. H., Wei, S. G., Francis, J., and Felder, R. B. 2003. Cardiovascular and renal sympathetic activation by blood-borne TNF-alpha in rat: the role of central prostaglandins. *Am J Physiol Regul Integr Comp Physiol* 284:R916.

32 Zhang, Z. H., Yu, Y., Wei, S. G., Nakamura, Y., Nakamura, K., and Felder, R. B. 2011. EP_3 receptors mediate PGE_2-induced hypothalamic paraventricular nucleus excitation and sympathetic activation. *Am J Physiol Heart Circ Physiol* 301:H1559.

33 Wilson, J., Higgins, D., Hutting, H. *et al.* 2013. Early propranolol treatment induces lung heme-oxygenase-1, attenuates metabolic dysfunction, and improves survival following experimental sepsis. *Crit Care* 17:R195.

34 Özyılmaz, E., Büyüknacar, H. S. G., Bağır, E. K. *et.al.*, 2019. Early propranolol treatment ameliorates endothelial dysfunction in experimental septic lung. *Adv Clin Exp Med* 28:291.

35 Neumann, B., Zantl, N., Veihelmann, A. *et al.* 1999. Mechanisms of acute inflammatory lung injury induced by abdominal sepsis. *Int Immunol* 11:217.

36 Muniz, B. F., Netto, G. M., Ferreira, M. J. *et al.* 2015. Neutrophilic infiltration in lungs of mice with peritonitis in acid or basic medium. *Int J Clin Exp Med* 8:5812.

37 Craciun, F. L., Schuller, E. R., and Remick, D. G. 2010. Early enhanced local neutrophil recruitment in peritonitis-induced sepsis improves bacterial clearance and survival. *J Immunol* 185:6930.

38 Burdon, P. C., Martin, C., and Rankin, S. M. 2008. Migration across the sinusoidal endothelium regulates neutrophil mobilization in response to ELR+CXC chemokines. *Br J Haematol* 142:100.

39 Takeda, S., Elefteriou, F., Levasseur, R. *et al.* 2002. Leptin regulates bone formation via the sympathetic nervous system. *Cell* 111:305.

40 Serre, C. M., Farlay, D., Delmas, P. D., and Chenu, C. 1999. Evidence for a dense and intimate innervation of the bone tissue, including glutamate-containing fibers. *Bone* 25:623.

Figure legends

Figure 1. Neutrophil egress was suppressed in denervated bone marrow under conditions of lipopolysaccharide (LPS)-induced inflammation.

(A–D) Intravital imaging analysis of lysozyme-M-enhanced green fluorescent protein (LysM-EGFP^{+}) cells in bone marrow chimeric mice after intraperitoneal LPS administration. Mice underwent superior cervical ganglionectomy (SCGx) or sham operation 10 days before the experiment. (A) Representative sequential intravital images 0, 30, 60, 90, and 120 minutes after LPS administration in the sham-operated group (upper panels) and sympathectomized group (lower panels). Images of the same visual field are shown. Vessels were visualized by intravenous injection of Qtracker 655. Blue, second harmonic generation (SHG). Green, LysM-EGFP^{+} cells; red, Qtracker 655. Scale bars, 100 μm. (B) Changes in the number of LysM-EGFP^{+} cells in the same visual field over time. The data are shown as number of cells relative to time 0 in each visual field (n = 4–7 visual fields from five independent experiments per group). (C) Time points of LysM-EGFP^{+} cell transmigration into the circulation during the 120-minute observation period (n = 163–230 from three independent experiments per group). The

data are means ± SEM. Statistical analyses were performed using the two-tailed *t* test (B) and Mann–Whitney U test (C) (*, $P < 0.05$; **, $P < 0.01$).

Figure 2. A β-adrenergic inhibitor suppressed C-X-C motif chemokine ligand 1 (CXCL1) expression in endothelial cells.

(A, B) Isolation of Lin^- $CD45^-$ $Sca\text{-}1^+$ $CD31^+$ endothelial cells, Lin^- $CD45^-$ $CD31^-$ mesenchymal cells, and $CD45^+$ leukocytes 2 hours after intraperitoneal LPS or phosphate-buffered saline (PBS) administration. Gating scheme (A) and expression of *Cxcl1* and *Cxcl2* in each cell type (B) ($n = 6$ per group). (C) Adrenergic receptor gene expression in endothelial cells under homeostatic conditions ($n = 4$). (D) Mice were treated intraperitoneally with 15 mg/kg propranolol (Pro) or vehicle 30 minutes before LPS administration, and endothelial cells were isolated 2 hours after LPS administration. *Cxcl1* and *Cxcl2* gene expression in endothelial cells is shown ($n = 4$ per group). The data are means ± SEM. Statistical analyses were performed using the two-tailed *t* test (B, D) and one-way ANOVA (C) (*, $P < 0.05$; ***, $P < 0.001$; ****, $P < 0.0001$; n.s., not significant).

Figure 3. Propranolol treatment inhibited neutrophil mobilization out of bone marrow and their accumulation in the lung.

(A–C) Intravital imaging analysis of LysM-EGFP^{+} cells in bone marrow after intraperitoneal injection of LPS. Mice were pretreated by intraperitoneal injection of 15 mg/kg propranolol (Pro) or vehicle 30 minutes before the experiment. (A) Representative sequential intravital images of parietal bone marrow 0, 30, 60, 90, and 120 minutes after LPS administration in vehicle-treated (upper panels) and propranolol-treated (Pro) mice (lower panels). Images of the same visual field are shown. Vessels were visualized by intravenous injection of Qtracker 655. Blue, SHG; green, LysM-EGFP^{+} cells; red, Qtracker 655. Scale bars, 100 μm. (B) Changes in the number of LysM-EGFP^{+} cells in the same visual field over time. The data are shown as number of cells relative to time 0 in each visual field ($n = 8$ visual fields from three independent experiments per group). (C) Time points of LysM-EGFP^{+} cell transmigration into the circulation during the 120-minute imaging period ($n = 93–103$ from three independent experiments per group). (D) Histological analysis of the

accumulation of LysM-EGFP^{+} cells in the lung after LPS or PBS administration. Mice were pretreated with propranolol or vehicle 30 minutes before LPS administration. Samples were collected 2 hours after LPS administration. Representative confocal images of lung sections from mice treated with PBS (left), LPS+vehicle (middle), and LPS+propranolol (Pro) (right); the densities of LysM-EGFP^{+} cells are shown in the right graph ($n = 9$ visual fields from three independent experiments per group). Blue, 4′,6-diamidino-2-phenylindole (DAPI); Green, LysM-EGFP^{+} cells; red, CD31. Scale bars, 100 μm. The data are means ± SEM. Statistical analyses were performed using the two-tailed *t* test (B, D) and Mann–Whitney U test (C) (*, $P < 0.05$; **, $P < 0.01$; ****, $P < 0.0001$; ns, not significant).

Figure 4. Scheme of the sympathetic neuronal regulation of neutrophil mobilization, mediated by CXCL1 production by endothelial cells.

At the onset of acute inflammation, the release of norepinephrine from the termini of sympathetic neurons increased, followed by upregulation of CXCL1 production by

endothelial cells, resulting in the promotion of neutrophil mobilization out of the bone marrow into the circulation.

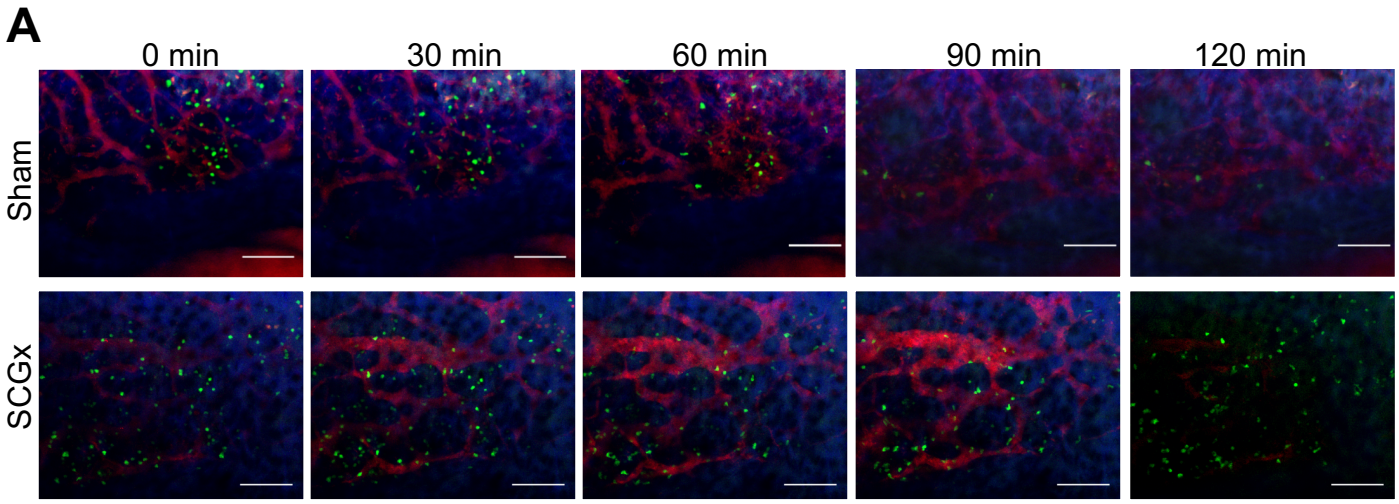
A
0 min
30 min
60 min
90 min
120 min
Sham
SCGx

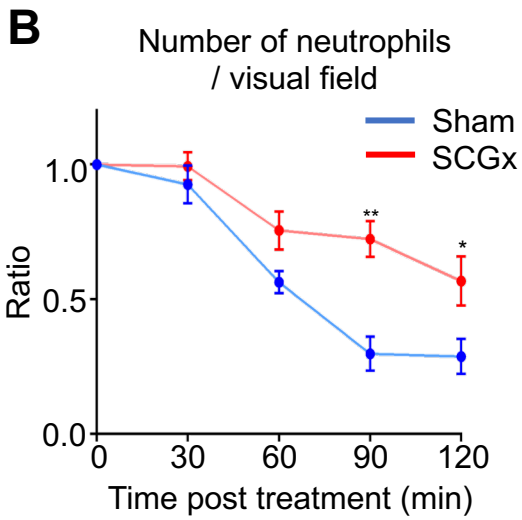
B
Number of neutrophils
/ visual field
Sham
SCGx
1.0
0.5
0.0
Ratio
**
*
0
30
60
90
120
Time post treatment (min)

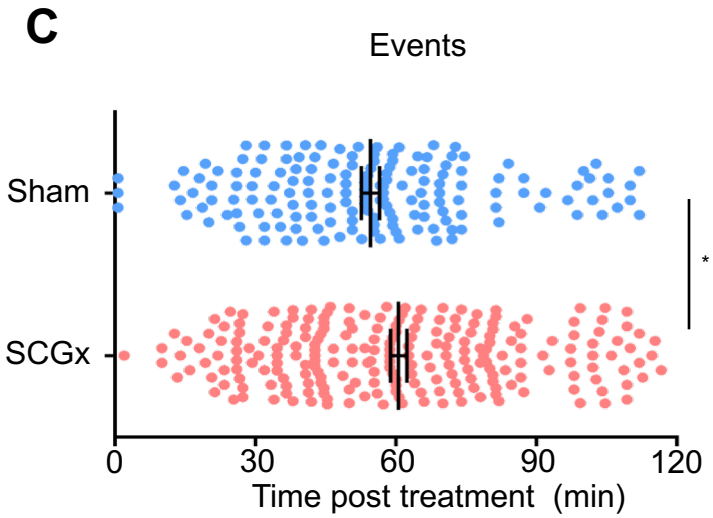
C
Events
Sham
SCGx
*
0
30
60
90
120
Time post treatment (min)

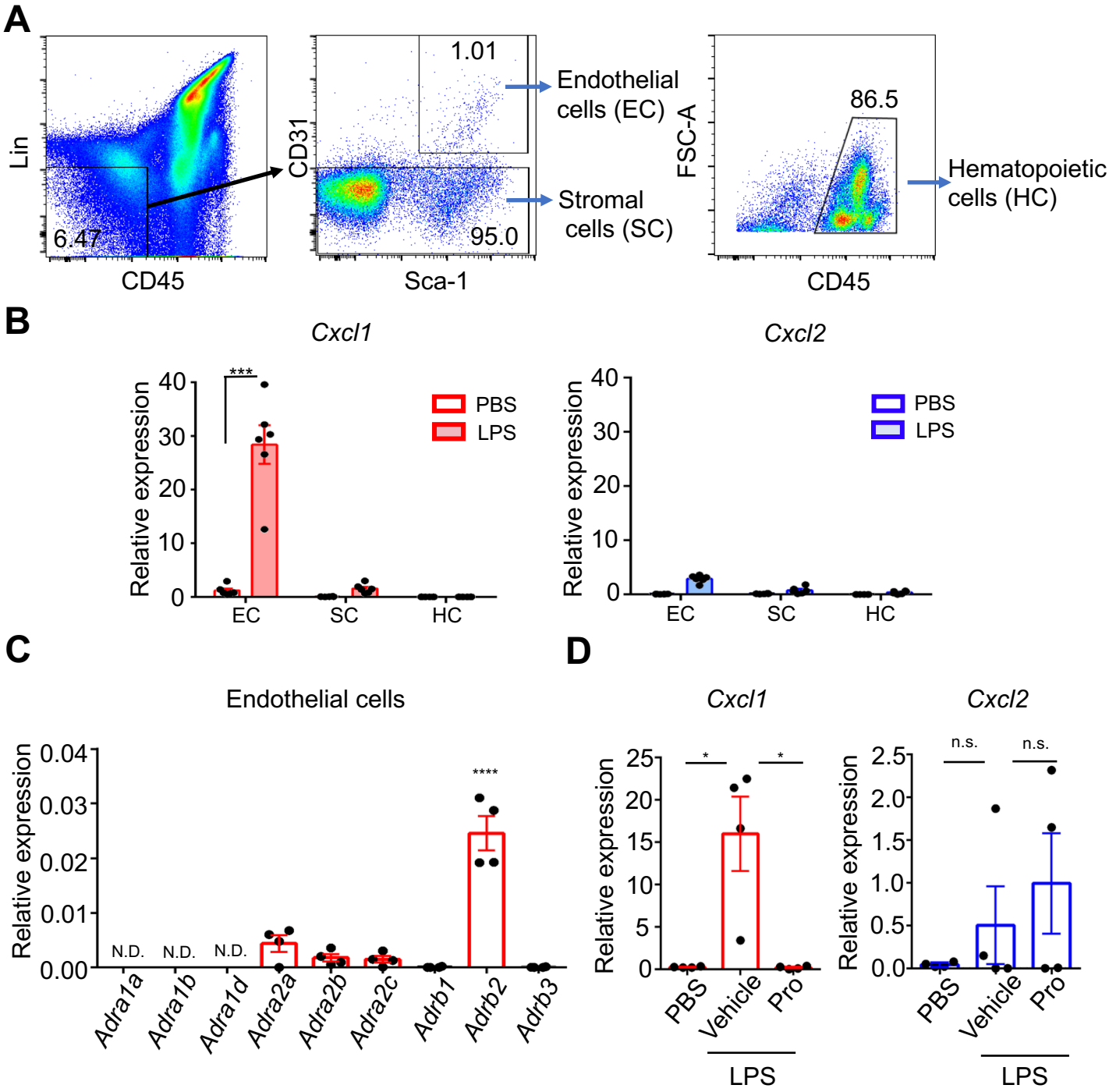
A
Lin
CD45
6.47
CD31
Sca-1
1.01
95.0
Endothelial cells (EC)
Stromal cells (SC)
FSC-A
CD45
86.5
Hematopoietic cells (HC)
B
Cxcl1
Cxcl2
Relative expression
PBS
LPS
***
EC
SC
HC
C
Endothelial cells
Relative expression
N.D.
****
Adra1a
Adra1b
Adra1d
Adra2a
Adra2b
Adra2c
Adrb1
Adrb2
Adrb3
D
Cxcl1
Cxcl2
Relative expression
*
n.s.
PBS
Vehicle
Pro
LPS

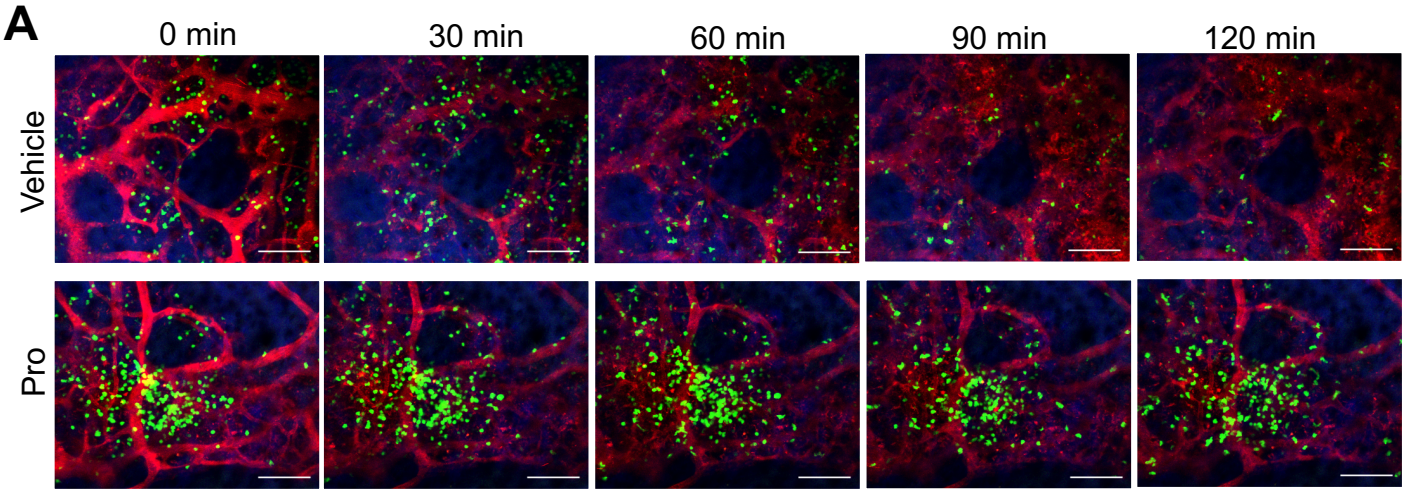
A
0 min
30 min
60 min
90 min
120 min
Vehicle
Pro

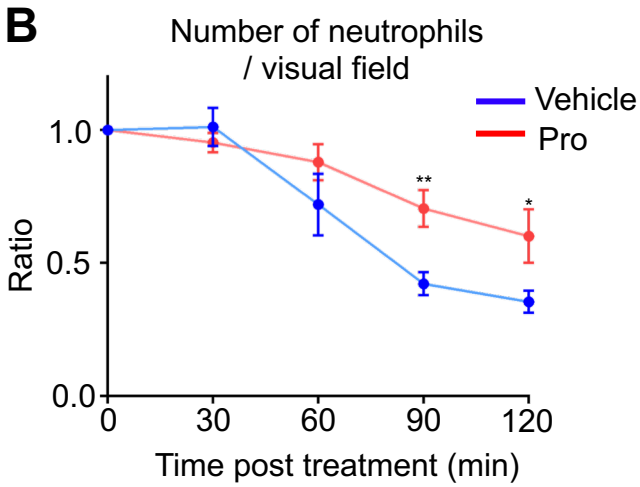
B
Number of neutrophils
/ visual field
Vehicle
Pro
Ratio
1.0
0.5
0.0
0
30
60
90
120
Time post treatment (min)
**
*

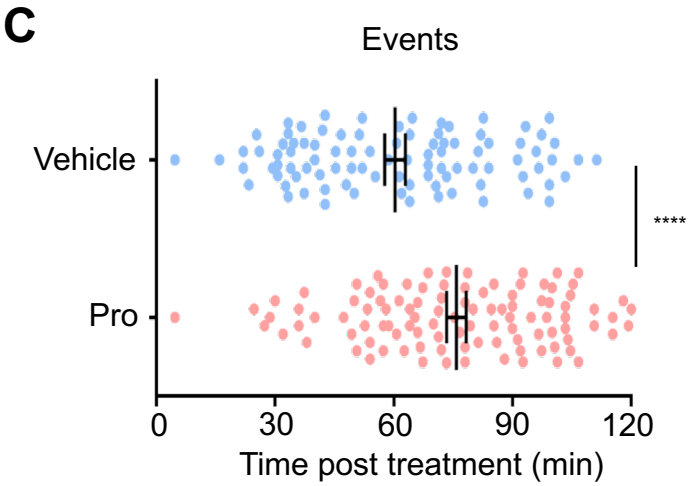
C
Events
Vehicle
Pro
****
0
30
60
90
120
Time post treatment (min)

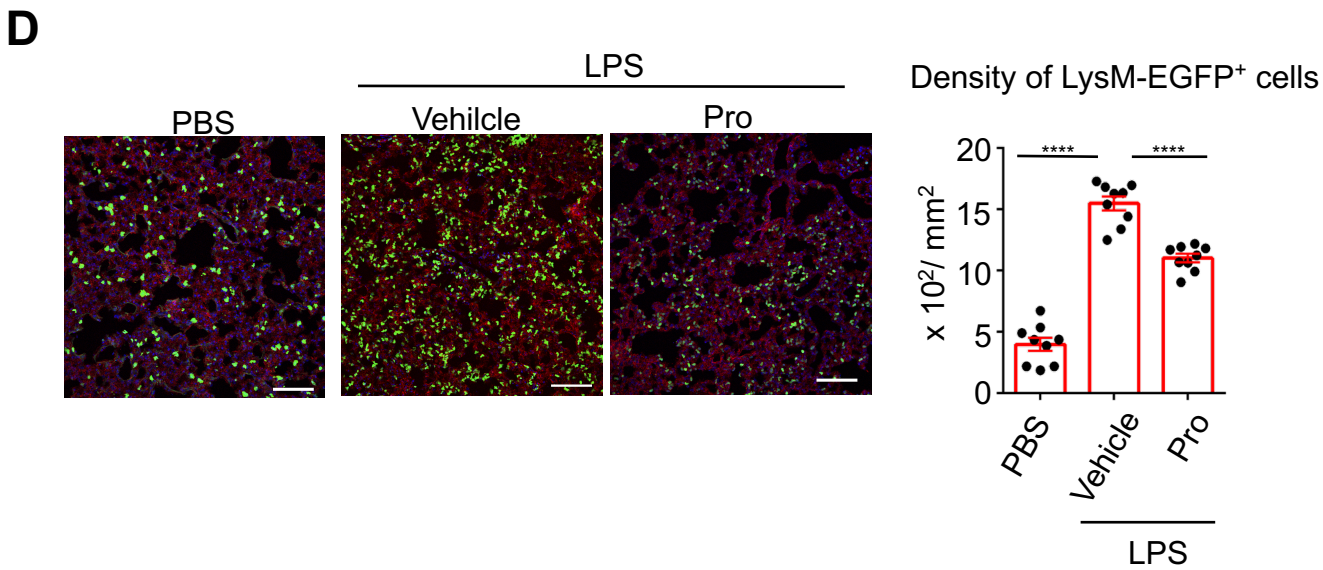
D
LPS
PBS
Vehilcle
Pro
Density of LysM-EGFP+ cells
x 10²/ mm²
20
15
10
5
0
****
****
PBS
Vehicle
Pro
LPS

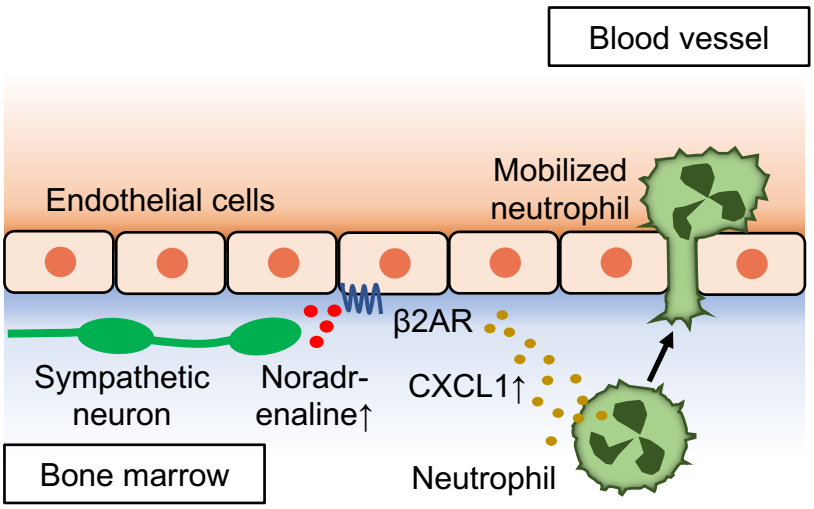
Blood vessel
Endothelial cells
Mobilized
neutrophil
β2AR
Sympathetic
neuron
Noradr-
enaline↑
CXCL1↑
Neutrophil
Bone marrow

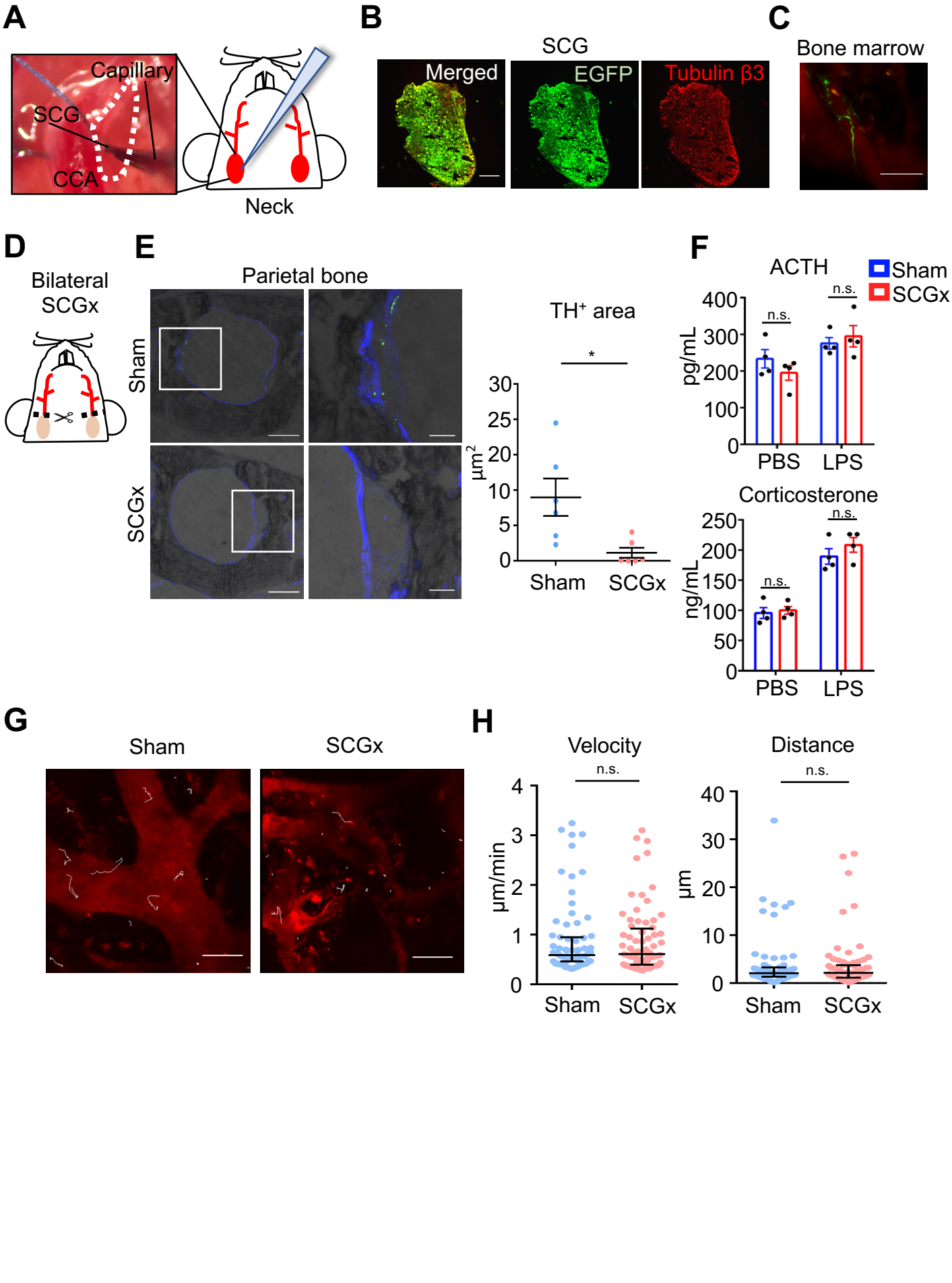
A
Capillary
SCG
CCA
Neck
B
SCG
Merged
EGFP
Tubulin β3
C
Bone marrow
D
Bilateral SCGx
E
Parietal bone
Sham
SCGx
TH+ area
*
μm2
30
25
20
10
5
0
Sham
SCGx
F
ACTH
Sham
SCGx
n.s.
n.s.
pg/mL
400
300
200
100
0
PBS
LPS
Corticosterone
n.s.
n.s.
ng/mL
250
200
150
100
50
0
PBS
LPS
G
Sham
SCGx
H
Velocity
n.s.
μm/min
4
3
2
1
0
Sham
SCGx
Distance
n.s.
μm
40
30
20
10
0
Sham
SCGx

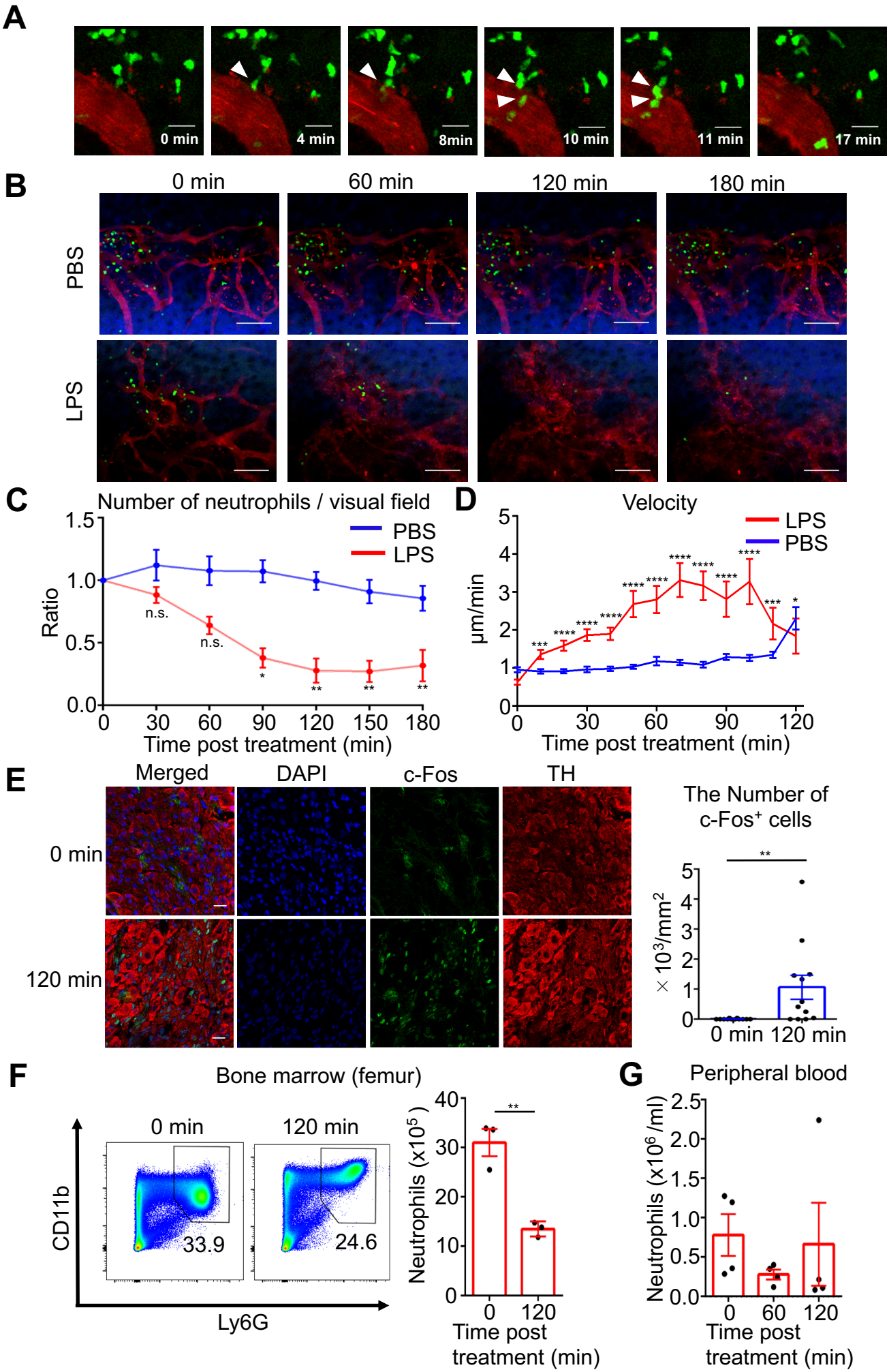
A
0 min
4 min
8min
10 min
11 min
17 min
B
0 min
60 min
120 min
180 min
PBS
LPS
C
Number of neutrophils / visual field
PBS
LPS
Ratio
n.s.
n.s.
Time post treatment (min)
D
Velocity
LPS
PBS
μm/min
Time post treatment (min)
E
Merged
DAPI
c-Fos
TH
0 min
120 min
The Number of c-Fos+ cells
× 10³/mm²
0 min
120 min
F
Bone marrow (femur)
0 min
120 min
CD11b
Ly6G
33.9
24.6
Neutrophils (x10⁵)
Time post treatment (min)
G
Peripheral blood
Neutrophils (x10⁶/ml)
Time post treatment (min)

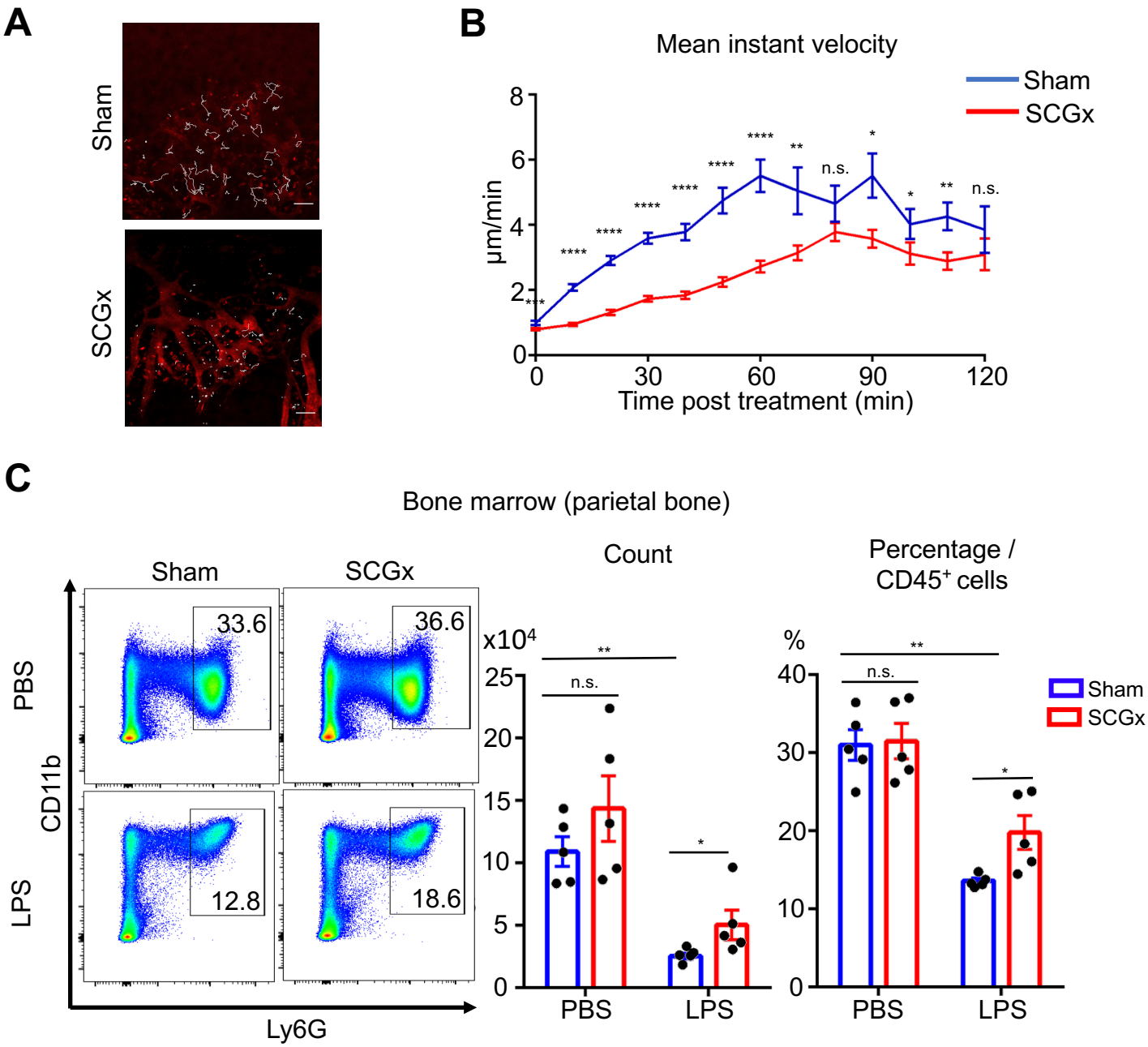
A
Sham
SCGx
B
Mean instant velocity
Sham
SCGx
µm/min
Time post treatment (min)
n.s.
C
Bone marrow (parietal bone)
Sham
SCGx
PBS
LPS
CD11b
Ly6G
33.6
36.6
12.8
18.6
Count
x10⁴
Percentage / CD45⁺ cells
%
n.s.
PBS
LPS

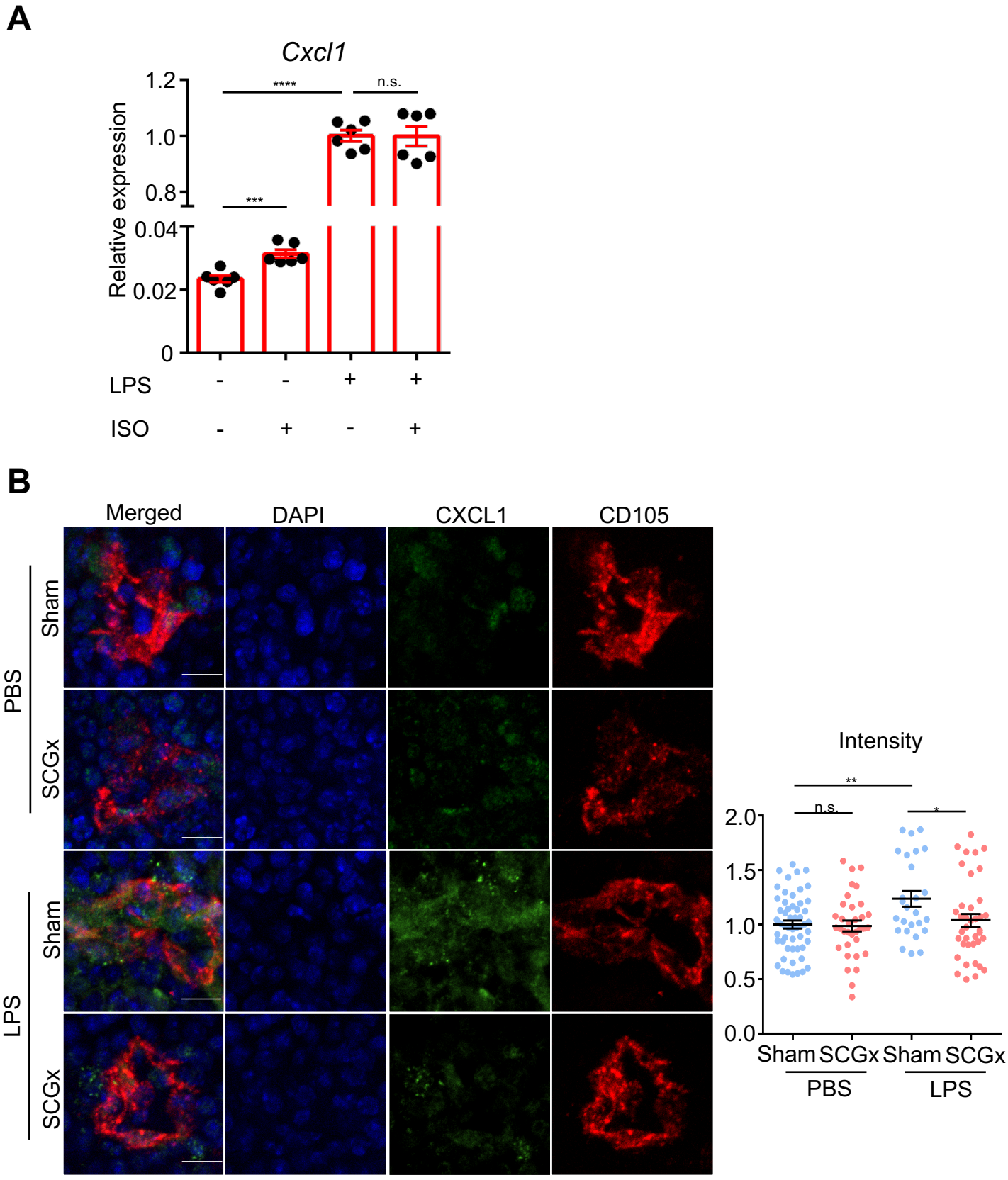
A
Cxcl1
Relative expression
1.2
1.0
0.8
0.04
0.02
0
****
n.s.
***
LPS
ISO
B
Merged
DAPI
CXCL1
CD105
PBS
LPS
Sham
SCGx
Intensity
2.0
1.5
1.0
0.5
0.0
**
n.s.
*
Sham
SCGx
Sham
SCGx
PBS
LPS

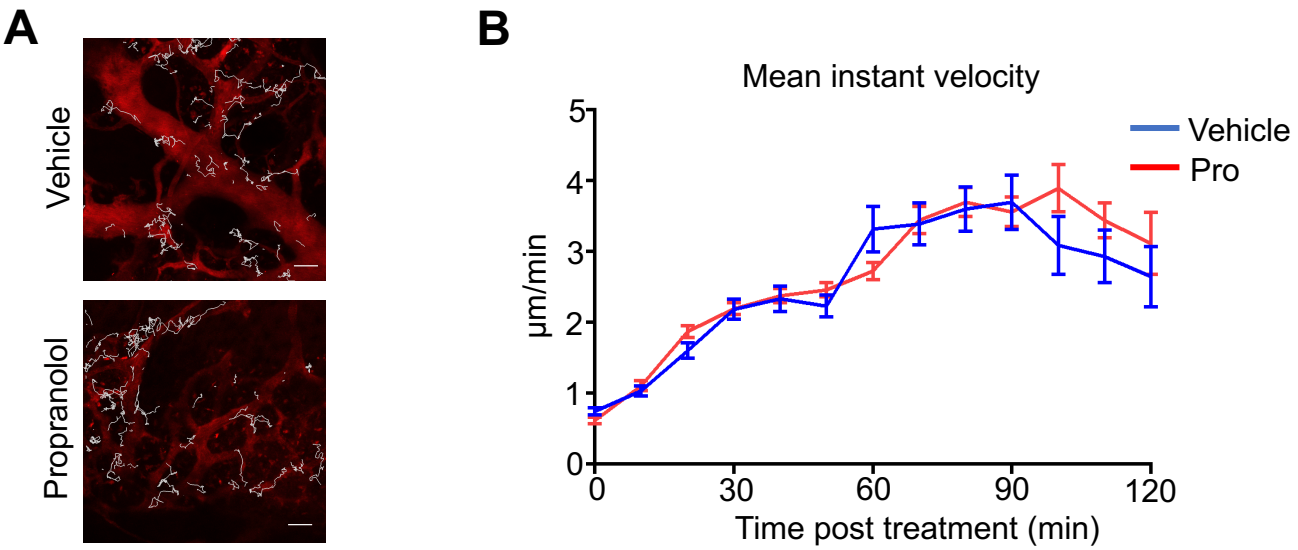
A
Vehicle
Propranolol
B
Mean instant velocity
Vehicle
Pro
µm/min
0
1
2
3
4
5
0
30
60
90
120
Time post treatment (min)

Table S1 Primers for real-time PCR

gene	primer	nucleotide sequence
Mouse *Gapdh*	forward	5-AGGTCGGTGTGAACGGATTTG-3′
	reverse	5′-TGTAGACCATGTAGTTGAGGTCA-3′
Mouse *Cxcl1*	forward	5′-TGTTGTGCGAAAAGAAGTGC-3′
	reverse	5′-CGAGACGAGACCAGGAGAAA-3′
Mouse *Cxcl2*	forward	5'-CCTGGTTCAGAAAATCATCCA-3′
	reverse	5'-CTTCCGTTGAGGGACAGC-3′
Mouse *Adra1a*	forward	5′-GCCCGGGGCTTTTATCCATGA-3′
	reverse	5′-GAAGATGTGGCCTCAGCCAG-3′
Mouse *Adra1b*	forward	5′-CTGGTCTTAGCTTCGTGGCA-3′
	reverse	5′-CTCGCTCGCCTCTAATGGG-3′
Mouse *Adra1d*	forward	5′-CAGGGACACAGAGTAGCAAGG-3′
	reverse	5′-TGAGGGAACAGAGAACCCAGAG-3′
Mouse *Adra2a*	forward	5′-TTTCCCCTGTGCCTAACTGC-3′
	reverse	5′-TGGCTTTATACACGGGGCTG-3′
Mouse *Adra2b*	forward	5′-GAGTCCAAGAAGCCCCATCC-3′
	reverse	5′-GGTGTCCATTAGCCTCTCCG-3′
Mouse *Adra2c*	forward	5′-AGGACTTCAGGCGCTCTTTC-3′
	reverse	5′-AGAGGGTCATTGCCTGAAGC-3′
Mouse *Adrb1*	forward	5'-GTGGGTAACGTGCTGGTGAT-3′
	reverse	5′-GAAGTCCAGAGCTCGCAGAA-3′
Mouse *Adrb2*	forward	5′-CAATAGCAACGGCAGAACGG-3′
	reverse	5′-TCAACGCTAAGGCTAGGCAC-3′
Mouse *Adrb3*	forward	5′-GGCCCTCTCTAGTTCCCAG-3′
	reverse	5′-TAGCCATCAAACCTGTTGAGC-3′
Human *ACTB*	forward	5′-CATGTACGTTGCTATCCAGGC-3′
	reverse	5′-CTCCTTAATGTCACGCACGAT-3′
Human *Cxcl1*	forward	5′-AGTCATAGCCACACTCAAGAATGG-3′
	reverse	5′-GATGCAGGATTGAGGCAAGC-3′
Human *Cxcl2*	forward	5′-CTCAAGAATGGGCAGAAAGC-3′
	reverse	5′-AAACACATTAGGCGCAATCC-3′